Analysis of tip-tilt compensation for reflective free-space optical satellite communication

Andreas Sinn, Thomas Riel, Peter Kremsner, and Georg Schitter

Automation and Control Institute (ACIN) TU Wien, Gusshausstrasse 27-29, 1040 Vienna, Austria

ABSTRACT

Atmospheric turbulences limit the achievable performance of free-space optical (FSO) satellite communication systems. Particularly in retro-reflective FSO satellite communication, tip-tilt disturbances are a dominant source of performance degradation and thus prevent the exploitation of the full potential of this communication system.

This publication investigates the total tip-tilt error of a terrestrial optical communication platform for reflective optical communication using a 14-inch telescope with tip-tilt compensation. The compensation system consists of a fast steering mirror (FSM), a quad photo diode (QPD) and a controller. Dynamic error budgeting is used to systematically analyze the system components' interplay and their contribution to the total error. Based on the results of the system analysis, a feedback controller for the compensation system is designed and tuned for disturbance rejection. The system's performance is evaluated with a reflective FSO communication link over a distance of 600 m in urban environment. The atmospheric aberration statistic is put into relation with comparable measurements using satellite to earth communication links. Measurement results successfully demonstrate the system's performance, effectively reducing the tip-tilt error up to a factor of 10.

Keywords: optical satellite communication, adaptive optics, tip-tilt compensation, dynamic error budgeting

1. INTRODUCTION

Free-space optical (FSO) satellite communication has become an important alternative to conventional radio frequency (RF) based communication systems. Over the last two decades a large number of projects demonstrated its potential for inter-satellite,[1–3] as well as satellite-earth communication.[4–7] All of the named systems require an active laser communication terminal (LCT) at the satellite, which provides a precision pointing mechanism, an optical antenna, as well as a laser source and a detector if applicable.[8,9] Although significant efforts to optimize this terminal in terms of space, weight and power (SWaP) have been made and the first commercial communication terminals for nano-satellites are available,[10] their applicability for pico- and nano-satellites may be limited. Limited actuation range of the LCT, as well as the power requirements for the laser source and the pointing system may exceed the restricted power budgets of pico- and nano-satellites and moving components introduce additional complexity, thus decreased operational time, of the satellite system.

To overcome these limitations but still be able to benefit form the potential of FSO communication and its growing network of OGS, reflective free-space optical (R-FSO) communication is a promising approach.[11] As shown in Figure 1 this principle replaces the active LCT with a modulating retro-reflector (MRR). The OGS tracks and illuminates the satellite's MRR with a laser beam. The retro-reflector ensures that the reflection is directed back to the transmitter without the need of an active pointing and tracking (PAT) system at the satellite. The reflected beam is modulated in terms of amplitude, polarization or phase to transmit information from the satellite to the OGS, of which intensity modulation with a transparent modulator type seems to be the most commonly used approach.[12–15] However, other approaches which modulate directly the retro-reflective property of the MRRv are currently investigated.[16,17] As all mechanical, complex and energy-consuming components are located at the OGS, operability, serviceability and life-time of the system are increased. The satellite provides energy for the modulator only. Due to its inherently compact and SWaP optimized principle its target application platform are mainly pico- and nano-satellites.

Further author information:
Andreas Sinn: E-mail: sinn@acin.tuwien.ac.at, Telephone: +43 1 58801 376 525.

Pre-print version of the article: A. Sinn, T. Riel, P. Kremsner, and G. Schitter, "Analysis of tip-tilt compensation for reflective free-space optical satellite communication," *Free-Space Laser Communications XXXI,* 109101G, 2019. DOI: 10.1117/12.2506472

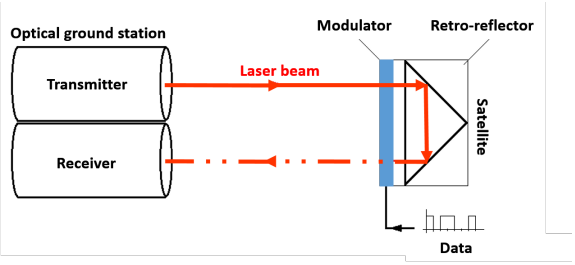

Figure 1. Principle of reflective free-space optical (R-FSO) communication. The optical ground station tracks and illuminates a modulating retro-reflector.

In the last few years several projects investigated the feasibility of R-FSO communication for pico- and nano-satellites. Several publications present promising link-budgets for satellites in low-earth-orbit (LEO),[18–21] as well as UAVs.[12,22] Verification measurements over various distances such as over a distance of 2 km at 2 Mbps,[23] 45 Mbps over a distance of 7 km[24] and 300 Mbps over a distance of 18.5 km[25] prove the potential of this technology.

As the laser beam propagates two times to the atmosphere, the influence of turbulence is increased significantly, resulting in the necessity of active wavefront correction strategies. To reduce the impact of atmospheric turbulence on this type of communication system and to maximize the amount of received photons at the OGS a precise, high-performance tip-tilt compensation system is required. This system enables the real-time compensation of atmospheric influences, as well as suppression of wind/vibration induced aberrations.[26] As tip-tilt aberrations contribute up to 80% of the RMS wavefront error in optical communication systems, high-performance compensation is essential.[27,28]

This publications presents the systematic analysis, implementation and verification of a high-performance tip-tilt compensation system for R-FSO communication. The used components are analyzed for their contributions to the total tip-tilt errors and measurements using an outdoor communication link in urban environment are presented.

2. SYSTEM DESCRIPTION

The investigated system is based on a bi-static telescope assembly consisting of a 356 mm Schmidt-Cassegrain telescope for reception (RX) and a 50 mm finder scope for transmission (TX). This assembly (Figure 5b) is mounted to an optical table for suppressing ground vibrations and is aligned in a way, that it faces a second building through free air distance of 300 m. A retro-reflector mounted on the second building is used as measurement target. This allows measurements over 600 m (two way distance) in urban environment.

An eye-safe semiconductor laser with a wavelength of 635 nm attached to the finder scope is used to illuminate the target retro-reflector (approx. 5 cm beam diameter). The bi-static approach separates the outgoing and incoming beam paths completely, effectively preventing internal reflections of the TX beam entering the RX path. As shown schematically in Figure 2, received light is collimated by lens L1 and directed via folding mirror M1 onto the FSM (OIM101, Optics in Motion LLC, Long Beach, California, USA). A relay lens assembly (L2 and L3) reduces the beam diameter to 10 mm to suite folding mirror M2. Another relay assembly (L4 and L5) further reduces the beam diameter to 1.1 mm for the wavefront sensor (WFS) (HASO 3 Fast, Imagine Optics, Orsay, France). A 50:50 beam splitter provides a second path where L4 and L6 form a third relay assembly. Lens L7 focuses the light of this path onto a custom made four quadrant photodetector (QPD) with integrating summing and subtraction amplifiers. QPD and FSM, as well as M2 and the WFS are located in conjugated planes. F1 is an optical bandpass filter which blocks ambient light. Names and descriptions of all optical components are summarized in Table 1. Signal acquisition and feedback control is implemented on a dSpace rapid prototyping system (DS1202, dSpace GmbH, Germany) in combination with Matlab. A sampling frequency of 25 kHz is used. The WFS is running with a frame-rate of 500 Hz and controlled by the Alpao Core Engine via Matlab.

Pre-print version of the article: A. Sinn, T. Riel, P. Kremsner, and G. Schitter, "Analysis of tip-tilt compensation for reflective free-space optical satellite communication," *Free-Space Laser Communications XXXI,* 109101G, 2019. DOI: 10.1117/12.2506472

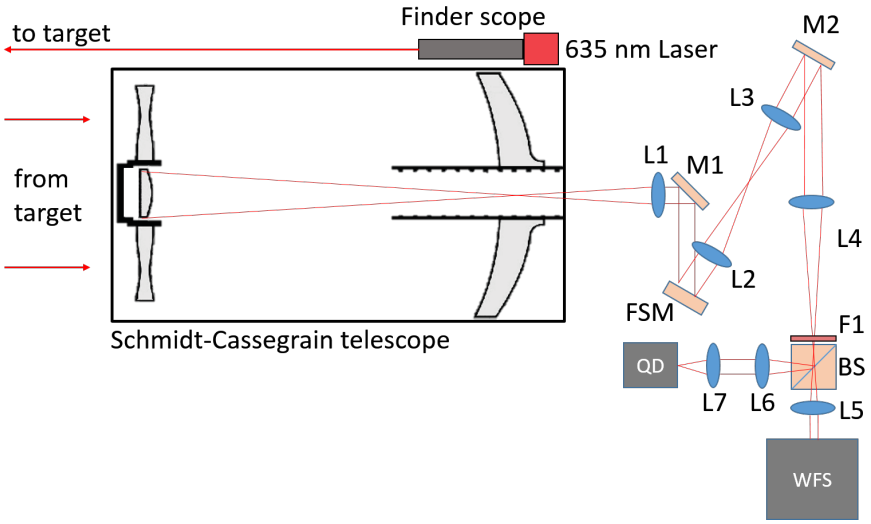

Figure 2. Sketch of the optical setup used for this publication (not to scale). A bi-static approach using a 356 mm telescope and a 5 cm finder scope is implemented.

3. SYSTEM ANALYSIS

The performance of the system is analyzed by means of dynamic error budgeting (DEB).[29] DEB is a tool to analyze the individual contributions of components in a system to the total output error. These components are modeled by LTI systems while stochastic disturbances are quantified by their power spectral densities (PSD).

3.1 Theoretical Background

A signal's noise power per unit of bandwidth can be quantified by its single-sided PSD.[30] Under the assumption of an unbiased time signal $w(t)$ its PSD corresponds to its variance by

$$\sigma_w^2 = \int_0^\infty \mathrm{PSD}_w(f)df, \tag{1}$$

where σ_w^2 is the variance of $w(t)$ and PSD_w the single-side PSD of $w(t)$. A specific disturbance $w(t)$ causes a corresponding $\mathrm{PSD}_{y,w}(f)$ at the output $y(t)$ of the system. This PSD is given by the propagation of $\mathrm{PSD}_w(f)$ through the transfer function $\mathrm{T}_{y,w}(f)$ from the disturbance to the output:

$$\mathrm{PSD}_{y,w}(f) = |T_{y,w}(f)|^2\,\mathrm{PSD}_w(f). \tag{2}$$

The overall PSD at the output y, assuming uncorrelated disturbances w_i, is superimposed by

$$\mathrm{PSD}_y(f) = \sum_i |T_{y,w_i}(f)|^2\,\mathrm{PSD}_{w_i}(f). \tag{3}$$

In order to clearly indicate the contribution of each disturbance source to the total output error the Cumulative Power Spectrum (CPS) is introduced by

$$\mathrm{CPS}(f) = \int_0^f \mathrm{PSD}(\nu)d\nu, \tag{4}$$

where $PSD(\nu)$ is a one-sided PSD.

Pre-print version of the article: A. Sinn, T. Riel, P. Kremsner, and G. Schitter, "Analysis of tip-tilt compensation for reflective free-space optical satellite communication," *Free-Space Laser Communications XXXI,* 109101G, 2019. DOI: 10.1117/12.2506472

Table 1. List of optical components and their properties used in the setup as presented in Figure 2.

Component	Name	Description
L1	Thorlabs LA1433-A	f = 150 mm
L2	Thorlabs LA1509-A	f = 100 mm
L3	Thorlabs LA1608-A	f = 75 mm
L4	Thorlabs AC254-300-A-ML	f = 300 mm
L5	Thorlabs LB1471A	f = 50 mm
L6	Thorlabs AC254-40-A-ML	f = 40 mm
L7	Thorlabs LB1761-A	f = 25.4 mm
M1	Thorlabs BB2-E02	D = 51 mm
M2	ALPAO DM69	D = 10 mm
BS	Thorlabs CM1-BS013	50:50 beam splitter
F1	Thorlabs FL05632.8-10	Line filter CWL = 632.8 nm, FWHM = 10 nm
FSM	Optics in Motion OIM101	D = 25 mm

3.2 Component Models

In this subsection the component's transfer functions, as well as the PSDs of the individual disturbance sources are derived. A schematic representation of the system with all modeled components and disturbances is shown in Figure 3a. Due to symmetric design and similar behavior of both axes (tip and tilt) identical models are used.

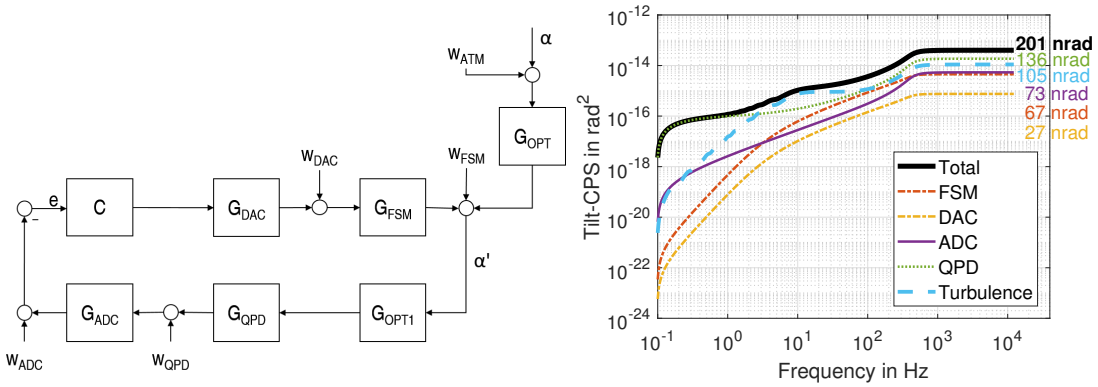

(a) (b)

Figure 3. System analysis overview. (a) Schematic representation of the compensation system including considered disturbance sources w_i, which are represented by their correspondent power spectral densities (PSD_i). (b) Result of the dynamic error budgeting analysis displayed as cumulative power spectrum of the tilt error. The values to the top right are the RMS values which are contributed by the individual components.

3.2.1 Analog/digital and digital/analog converters

The analog inputs of the used rapid prototyping platform provide 16 bit resolution at an input voltage range of ±10 V and a sampling rate of 25 kHz. All input channels are equipped with anti-aliasing filters using first order low-pass filters with a cutoff frequency of 10 kHz. The quantization noise σ_{ADCq}, modeled as unbiased white

Pre-print version of the article: A. Sinn, T. Riel, P. Kremsner, and G. Schitter, "Analysis of tip-tilt compensation for reflective free-space optical satellite communication," *Free-Space Laser Communications XXXI,* 109101G, 2019. DOI: 10.1117/12.2506472

noise which is distributed equally up to the Nyqist frequency f_N (as shown in Ref. 30), is given by

$$\sigma^2_{ADCq} = \frac{\mathrm{LSB0}^2_{ADC}}{12} \tag{5}$$

where LSB_{ADC} specifies the voltage of the least significant bit. Measurements quantify the electric noise to be $\sigma_{ADCe} = 0.7$ mV RMS. Since these noise sources are uncorrelated the total ADC noise is the sum of the variances

$$\sigma^2_{ADC} = \sigma^2_{ADCq} + \sigma^2_{ADCe}. \tag{6}$$

The PSD of the ADC is calculated by following equation

$$\mathrm{PSD}_{ADC}(s) = |G_{ADC}(s)|^2 \, \frac{\sigma^2_{ADC}}{f_N}, \tag{7}$$

with G_{ADC} being the transfer function of the first order low-pass filter and f_N the Nyquist frequency.

Similar to the ADC the analog output channels have a resolution of 16 bit at an output voltage range of ±10 V. The output sample frequency is 25 kSps and first order low-pass filters with a cutoff frequency of 10 kHz are used as reconstruction filters. The quantization noise σ_{DACq}, with LSB_{DAC} as the voltage of the least significant bit, is given by

$$\sigma^2_{DACq} = \frac{\mathrm{LSB}^2_{DAC}}{12}. \tag{8}$$

The electrical noise of the DAC is measured to $\sigma_{DACe} = 0.12$ mV RMS. The PSD of the DAC is calculated by

$$\mathrm{PSD}_{DAC}(s) = |G_{DAC}(s)|^2 \, \frac{\sigma^2_{DACq} + \sigma^2_{DACe}}{f_N}, \tag{9}$$

where G_{DAC} is the transfer function of the low-pass filter.

3.2.2 Fast steering mirror

The FSM is an assembly of an OIM101 tip-tilt mirror in combination with custom made, analog PI current controllers (based on OPA549TG, Texas Instruments Inc, Dallas, USA), providing a mechanical actuation range of ±26.2 mrad for both axes. Its transfer functions are shown in Figure 4. Typical behavior of a mass-spring-damper system with the suspension mode at 27 Hz can be observed.[31] Both axes show identical frequency response, therefor only one model is used for both axes. A second order model as derived in Ref. 31 is used to characterize the frequency response. Its measured PSD is given by

$$\mathrm{PSD}_{FSM}(s) = |G_{FSM}(s)|^2 \left| \frac{s + 2\pi \cdot f_{FSM_e}}{s + 2\pi \cdot f_{FSM_s}} \right|^2 \frac{\sigma^2_{FSM}}{F_N}, \tag{10}$$

where G_{FSM} is the fitted transfer function of the FSM, $\sigma^2_{FSM} = 0.748$ mV its RMS noise and $f_{FSM_s} = 0.1$ Hz and $f_{FSM_e} = 1$ Hz the frequencies specifying 1/f noise.

3.2.3 Tip-tilt sensor

Tip-tilt aberrations are measured with a custom made QPD circuit. This circuit includes transimpedance amplifiers, as well as summing and subtraction amplifiers and delivers tip, tilt and sum outputs. Its frequency response is modeled by a combination of a first order low-pass filter for the photo-detector and TIA and a second order low-pass filter for the summing/subtracting amplifiers. The frequency behavior of the TIA is mainly defined by the feedback resistance R_f and the junction capacitance C_j of the photo-detector. Its -3-dB cutoff frequency is calculated with

$$f_{3dB,TIA} = \sqrt{\frac{\mathrm{GBW}}{4\pi R_f C_j}}. \tag{11}$$

Pre-print version of the article: A. Sinn, T. Riel, P. Kremsner, and G. Schitter, "Analysis of tip-tilt compensation for reflective free-space optical satellite communication," *Free-Space Laser Communications XXXI,* 109101G, 2019. DOI: 10.1117/12.2506472

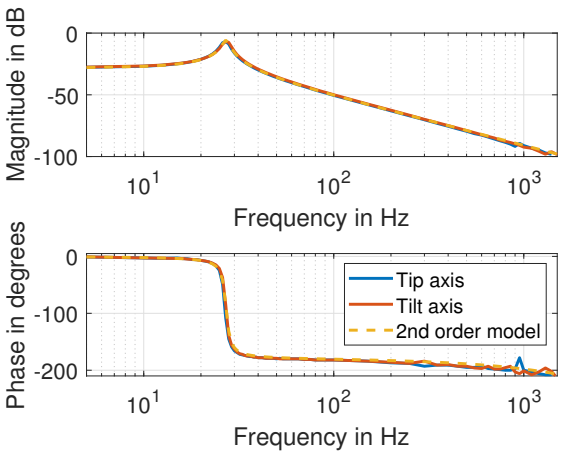

Figure 4. System analysis results. (a) Bode diagram of both axes of the FSM, which show similar behavior over the displayed frequency range. The yellow line indicates a fitted second order model with a resonance frequency of 27 Hz.

The summing and subtracting amplifiers have integrated second order low-pass filters with a -3-dB cutoff frequency of 8 kHz. The dynamics of the QPD are given by

$$G_{QPD}(s) = k_{QPD} \cdot G_{TIA}(s) \cdot G_{SUM/SUB}(s), \tag{12}$$

where G_{TIA} and $G_{SUM/SUB}$ are the transfer functions of the TIA and the summing/subtracting amplifiers and k_{QPD} includes all gains from the amplifiers as well as the position sensitivity of the QPD. This factor is measured to $k_{QPD} = 788$. To include low frequency noise a combination of 1/f-noise with a corner frequency $f_{1/f,QPD}$ and white noise is used. The corner frequency is identified by measurement to $f_{1/f,QPD} = 1$ Hz. The resulting PSD is given by

$$\mathrm{PSD}_{QPD}(s) = |G_{QPD}(s)|^2 \cdot \left| \frac{s + 2\pi \cdot f_{1/f,QPD}}{s} \right|^2 \frac{\sigma_{QPD}^2}{F_N}. \tag{13}$$

3.2.4 Optical setup

The optical system reduces the incoming beam diameter from 356 mm to 15 mm on the FSM. This amplifies the angle of arrival fluctuations by a factor of $k_{OPT} = 24$. Therefor, the temporal transfer function of the optical system is given by a constant gain

$$G_{OPT}(s) = k_{OPT}. \tag{14}$$

The same accounts for the second reduction of the beam diameter from 15 mm to 1.6 mm to suite the WFS, which results in a constant gain of $k_{OPT1} = 9.4$

$$G_{OPT1}(s) = k_{OPT1}. \tag{15}$$

3.2.5 Atmosphere

To get an estimation of the tip-tilt PSD of due to atmospheric turbulence the a parametric Hufnagel-Valley model HV5/7 is used.[32] It is representative for a vertical optical communication channel under quite harsh seeing conditions. Following equation (16) is used to determine the PSD[33]

$$\mathrm{PSD}_{tilt}(f) = 0.155 \cdot D^{-\frac{1}{3}} \cdot sec(\alpha) \cdot f^{-\frac{8}{3}} \int C_n^2(h) \cdot (V(h))^{5/3} \cdot F_g \left(\frac{f}{V(h)} \right) dh, \tag{16}$$

Pre-print version of the article: A. Sinn, T. Riel, P. Kremsner, and G. Schitter, "Analysis of tip-tilt compensation for reflective free-space optical satellite communication," *Free-Space Laser Communications XXXI,* 109101G, 2019. DOI: 10.1117/12.2506472

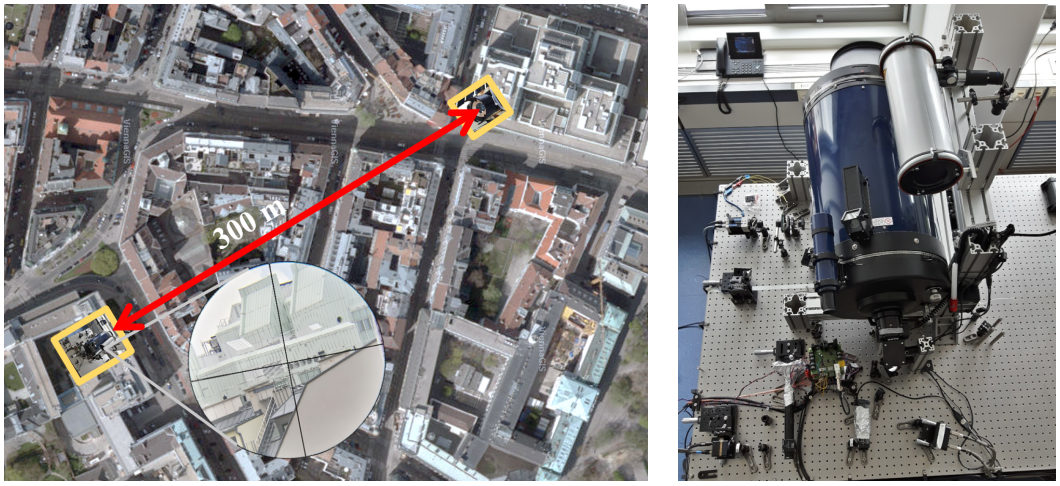

(a) (b)

Figure 5. Experimental system overview. (a) Aerial view of the optical communication path between two buildings of TU Wien (data source: City of Vienna - data.wien.gv.at). The single way distance is 300 m. (b) Image of the optical system. The silver telescope on the right top is not used in this publication.

where f is the temporal frequency, D is the diameter of the telescope, α the zenith angle, $C_n^2(h)$ the refractive index structure function, V(h) is the wind profile as a function of the height and F_g the G-tilt Greenwood frequency as defined in.[33] The calculated PSD is shown in Figure 7.

3.2.6 Controller

A tamed PID controller is designed for closed-loop operation of the tip-tilt compensation system.[29] Its frequency response is given by

$$C(s) = K_p + \frac{K_i}{s} + \frac{K_d s}{\tau_t s + 1}, \tag{17}$$

with K_p as proportional, K_i as integral and K_d as derivative controller gains. A filter with the time constant τ_t limits the differentiating action at higher frequencies. Its gains are calculated based on the open-loop frequency response of the full system. A closed loop bandwidth of 512 Hz is achieved.

3.3 Simulation Results

Using the LTI system models, as well as the PSDs derived in the previous subsection, the expected performance of the tip-tilt compensation system is estimated by means of dynamic error budgeting. Using the transfer functions from each disturbance source to the output α' in Equation 3 leads to the total PSD of α'. In order to allow reasonable comparison of the achieved performance with other systems, the output α' is scaled by the gain of the optical system (G_{OPT}), which is equivalent to the angle of arrival α in front of the telescope. This output is shown in form of a CPS in Figure 3b. A total error of 201 nrad is estimated. Compared to the results of a similar system analyzed in Ref. 26, the individual disturbance source's contributions are located in a similar region (especially QPD, ADC, and FSM). This indicates that the system is close to its optimal performance and further improvement would necessitate the optimization of at least three components.

4. EXPERIMENTAL RESULTS

To verify the results of the system analysis, measurements between two buildings of TU Wien over a distance of 600 m are performed. An aerial view of the communication path is given in Figure 5a. This link is exposed to the (in terms of optical turbulence) harsh urban environment of Vienna, resulting in a representative scenario for system evaluation.

Pre-print version of the article: A. Sinn, T. Riel, P. Kremsner, and G. Schitter, "Analysis of tip-tilt compensation for reflective free-space optical satellite communication," *Free-Space Laser Communications XXXI,* 109101G, 2019. DOI: 10.1117/12.2506472

4.1 Channel Characterization

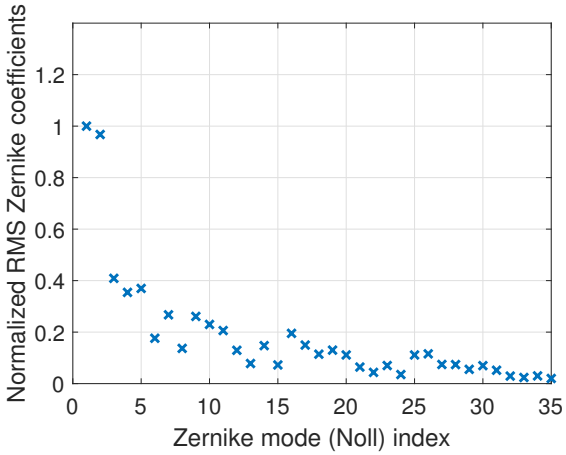

Figure 6. Aberration statistic of the used R-FSO channel over 600 m in urban environment. 10000 frames are recorded by the WFS and used for calculation. The RMS coefficients are normalized for comparison and static aberrations have been removed. Tip-tilt contributes by far the most to the total error.

To qualify the optical channel its aberration statistic is recorded with a wavefront sensor and compared to values from literature. The WFS is running with a frame-rate of 500 Hz for a measurement duration of 20 s. The reference light source for the WFS is the laser of the R-FSO communication setup. The measurements represent the conditions of a typical summer night (no clouds, no fog, no rain) with an ambient temperature of 23 °C, a relative humidity of 52% and an average wind speed of 5.6 $\frac{m}{s}$. The result of this measurement is shown in Figure 4.1. Noll's notation is used to decompose the received wavefronts into aberration types.[34] Static aberrations (due to imperfections of the optical system) have been removed for this plot. A significant dominance of tip-tilt aberrations is visible, which is typical for free-space optical communication systems.[35] An angle of arrival error of approximately 2.1 µrad for the tip and 2.0 µrad for the tilt axis is observed in this measurement. According to Ref. 36 an angle of arrival variation under average seeing conditions ($r_0 = 12$ cm) of 1.9 µrad RMS is estimated.

For evaluation of the temporal characteristics of the channel its power spectral density is put into relation by a vertical channel using again the HV5/7 model. Figure 7 shows the measured tip-tilt power spectral densities without and with compensation and the calculated HV5/7 tip-tilt PSD. Both the uncompensated channel and the HV5/7 model show similar behavior, confirming the used R-FSO link to be a representative scenario for system verification.

4.2 System verification

With known channel properties and a simulated estimation of the systems performance verification measurements using the full tip-tilt compensation system are executed. The retro-reflector is illuminated by the laser via the finder scope and the reflected beam is collected with the Schmidt-Cassegrain telescope and directed into the optical system. Two consecutive measurements are performed within one minute to ensure constant atmospheric properties acting on the R-FSO communication link. The measurement results again are transformed to the input of the telescope (using the magnification of the optical system). The first measurement with a duration of 30 s is taken as reference with disabled tip-tilt compensation. The PSD of this measurement is shown in Figure 7 for both tip and tilt axes. It is, as stated previously, in good agreement to the used HV5/7 model based comparison link.

After 30 s the tip-tilt compensation is enabled, resulting in an immediate decrease of the tip and tilt errors by up to a factor of 10 to 290 nrad RMS for the tip (Fig. 7a) and 210 nrad RMS for the tilt axis (Fig. 7b). This

Pre-print version of the article: A. Sinn, T. Riel, P. Kremsner, and G. Schitter, "Analysis of tip-tilt compensation for reflective free-space optical satellite communication," *Free-Space Laser Communications XXXI,* 109101G, 2019. DOI: 10.1117/12.2506472

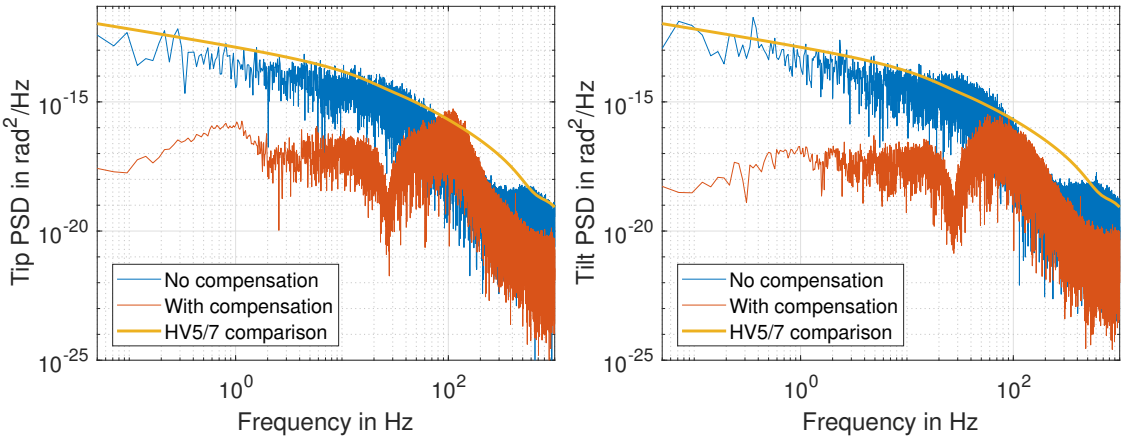

(a) (b)

Figure 7. Temporal tip (a) and tilt (b) power spectra of the system's output measured with the QPD. A clear reduction of the measured error below 100 Hz is shown. The yellow lines indicate the calculated PSD for a vertical link using a HV5/7 model.

behavior is also clearly visible in the time signals shown in Figure 8. The performance of the system is in good agreement with the results from the system analysis, not only proving DEB as powerful tool for analysis and optimization, but also clearly demonstrating the improvement due to a high performance tip-tilt compensation system.

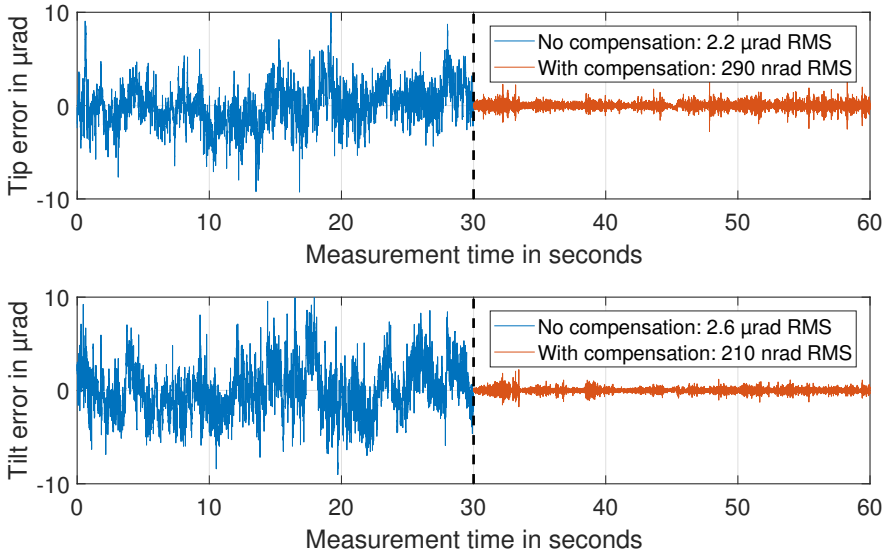

Figure 8. Time signal of tip and tilt error measured by the QPD. After 30 s tip-tilt compensation is enabled, drastically reducing the error by up to a factor of ten.

Pre-print version of the article: A. Sinn, T. Riel, P. Kremsner, and G. Schitter, "Analysis of tip-tilt compensation for reflective free-space optical satellite communication," *Free-Space Laser Communications XXXI,* 109101G, 2019. DOI: 10.1117/12.2506472

5. CONCLUSION

This publication presents the systematic analysis of an exemplary communication system in terms of tip-tilt compensation. Dynamic error budgeting is used to estimate the performance of the system. Models of the components are derived and used to study the contributions of the individual disturbance sources to the total system performance. The analysis predicts an achievable tip-tilt error of 201 nrad RMS. Verification measurements over a link distance of 600 m using a reflective communication setup in urban environment, successfully demonstrate the reduction of the tip-tilt error by a factor of 10 to 290 nrad RMS in the tilt and 210 nrad RMS in the tip axis. The measured aberration statistic of this channel shows similar distribution of aberrations when compared to literature and is therefore considered as valid channel for verification measurements.

ACKNOWLEDGMENTS

The authors gratefully acknowledge the excellent cooperation with ASA Astrosysteme GmbH and thank for its support and valuable expertise.

This work was funded by the Austrian Ministry for Transport, Innovation and Technology (BMVIT) under the scope of the Austrian Space Applications Program (FFG project number 854050).

REFERENCES

[1] Toyoshima, M., Yamakawa, S., Yamawaki, T., Arai, K., Yabe, K., and Shiratama, K., "Reconfirmation of the optical performances of the laser communications terminal onboard the OICETS satellite," *Acta Astronautica* **55**(3-9), 261–269 (2004).

[2] Smutny, B., Kaempfner, H., Muehlnikel, G., Sterr, U., Wandernoth, B., Heine, F., Hildebrand, U., Dallmann, D., Reinhardt, M., Freier, A., Lange, R., Boehmer, K., Feldhaus, T., Mueller, J., Weichert, A., Greulich, P., Seel, S., Meyer, R., and Czichy, R., "5.6 Gbps optical intersatellite communication link," in [*Proc. SPIE 7199, Free-Space Laser Communication Technologies XXI*], (719906) (2009).

[3] Arora, H. and Goyal, R., "A Review on Inter-satellite Link in Inter-satellite Optical Wireless Communication," *Journal of Optical Communications* **38**(1), 63–67 (2017).

[4] Giggenbach, D., Epple, B., Horwath, J., and Moll, F., "Optical satellite downlinks to optical ground stations and high-altitude platforms," *Lecture Notes in Electrical Engineering* **16**, 331–349 (2008).

[5] Gregory, M., Heine, F., Kämpfner, H., Meyer, R., Fields, R., and Lunde, C., "TESAT laser communication terminal performance results on 5.6Gbit coherent inter satellite and satellite to ground links," *International Conference on Space Optics — ICSO 2010* **10565**(October), 37 (2017).

[6] Kaushal, H. and Kaddoum, G., "Free Space Optical Communication: Challenges and Mitigation Techniques," *IEEE Communications Surveys & Tutorials* **19**(1), 57–96 (2017).

[7] Kolev, D. R. and Toyoshima, M., "Satellite-to-ground optical communications using small optical transponder (SOTA) – received-power fluctuations," *Optics Express* **25**(23), 28319 (2017).

[8] Janson, S., Welle, R., Rose, T., Rowen, D., Hardy, B., Dolphus, R., Doyle, P., Faler, A., Chien, D., Chin, A., Maul, G., Coffman, C., Lumondiere, S. D. L., Nicolette, I., and Hinkley, D., "The NASA Optical Communications and Sensor Demonstration Program : Initial Flight Results," *29th Annual AIAA/USU Conference on Small Satellities* **3**(3), 1–8 (2016).

[9] Carrasco-Casado, A., Harrison, F., Biswas, A., Fields, R., Grefenstette, B., Harrison, F., Sburlan, S., and Toyoshima, M., "Optical Communication on CubeSats - Enabling the Next Era in Space Science," in [*IEEE International Conference on Space Optical Systems and Applications (ICSOS) 2017*], 46–52 (2017).

[10] TESAT SPACECOM, "CUBE-LCT Smallest laser communication transmitter worldwide," (2018).

[11] Jensen, G. and Swenson, C., "A Laser Downlink for Small Satellites Using an Optically Modulating Retroreflector," in [*Small satellite conference*], 10 (1992).

[12] Swenson, C. M., Steed, C. a., Delarue, I. a., and Fugate, R. Q., "Low Power FLC-based Retromodulator Communications System," *SPIE Free-Space Laser Communication Technologies IX* **2990** (1997).

[13] Rabinovich, W. S., Mahon, R., Goetz, P. G., Waluschka, E., Katzer, D. S., Binari, S. C., and Gilbreath, G. C., "A cat's eye multiple quantum-well modulating retro-reflector," *IEEE Photonics Technology Letters* **15**(3), 461–463 (2003).

Pre-print version of the article: A. Sinn, T. Riel, P. Kremsner, and G. Schitter, "Analysis of tip-tilt compensation for reflective free-space optical satellite communication," *Free-Space Laser Communications XXXI,* 109101G, 2019. DOI: 10.1117/12.2506472

[14] Sjöqvist, L., Hard, S., and Juniqe, S., "Retroreflective Free-Space Optical Communication. System and Performance Analysis," Tech. Rep. FOI-R–0344–SE, Swedish Defence Research Agency, Division of Sensor Technology (2001).

[15] Majumdar, A. K., [*Advanced Free Space Optics*], Springer Science, New York (2015).

[16] Ziph-Schatzberg, L., Bifano, T., Cornelissen, S., Stewart, J., and Bleier, Z., "Secure optical communication system utilizing deformable MEMS mirrors," in [*Proceedings Volume 7209, MEMS Adaptive Optics III*], **7209**, 7209 – 7209 – 15 (2009).

[17] Schultz, P., Cumby, B., and Heikenfeld, J., "Investigation of five types of switchable retroreflector films for enhanced visible and infrared conspicuity applications," *Applied Optics* **51**(17), 3744 (2012).

[18] Sinn, A., Riel, T., Deisl, F., Saathof, R., and Schitter, G., "Low-Power Reflective Optical Communication System for Pico- and Nano-Satellites," in [*Proceedings of the Advanced Maui Optical and Space Surveillance Technologies Conference*], 1403 – 1410 (2016).

[19] Gouy, Y., Steck, E., Sanchez, C., Faulkner, G., O'Brien, D., and Sproll, F., "The C3PO project: a laser communication system concept for small satellites," in [*Proc. SPIE 10096, Free-Space Laser Communication and Atmospheric Propagation XXIX*], (March), 141–144 (2017).

[20] Stupl, J., Salas, A. G., Wu, S., Arbitman, D., Tilles, J., and Lucas, C. R. D., "Modulating Retro-Reflector Cubesat Payload operating at 1070nm for Asymmetric Free-space Optical Communications," (2016).

[21] Salas, A., Stupl, J., and Mason, J., "Modulating Retro-Reflectors: Technology, Link Budgets and Applications," in [*63rd International Astronautical Congress*], 1–6 (2012).

[22] Rabinovich, W., Gilbreath, G., Bovais, C., Cochrell, K., Burris, H., Ferraro, M., Vilcheck, M., Mahon, R., Goins, K., Sokolsky, I., Vasquez, J., Meehan, T., Barbehehn, R., Katzer, D., and Ikossi-Ansatasiou, K., "Infrared data link using a multiple quantum well modulating retro-reflector on a small rotary-wing UAV," *2000 IEEE Aerospace Conference. Proceedings* **3** (2000).

[23] Goetz, P. G., Rabinovich, W. S., Mahon, R., Ferraro, M. S., Murphy, J. L., Burris, H. R., Stell, M. F., Moore, C. I., Suite, M. R., Freeman, W., Gilbreath, G. C., and Binari, S. C., "Modulating retro-reflector devices and current link performance at the naval research laboratory," in [*Proceedings - IEEE Military Communications Conference MILCOM*], 1–7 (2007).

[24] Rabinovich, W. S., Goetz, P. G., Mahon, R., Swingen, L., Murphy, J., Ferraro, M., Burris, H. R., Moore, C. I., Suite, M., Gilbreath, G. C., Binari, S., and Klotzkin, D., "45-Mbit/s cat's-eye modulating retroreflectors," *Optical Engineering* **46**(October), 104001 (2007).

[25] Rabinovich, W., Moore, C., Mahon, R., Murphy, J. L., Thomas, L. M., and Gilbreath, G. C., "Free-space optical communications research and demonstrations at the U. S. Naval Research Laboratory," *Applied Optics* **54**(31), F189–F200 (2015).

[26] Sinn, A., Riel, T., Deisl, F., and Schitter, G., "Tip-Tilt Vibration Compensation: A system Analysis," in [*Proceedings of ASPE 2017 Spring Topical Meeting - Precision Engineering and Optics: What are the Limits of Precision, and How to Characterize Them?*], 42–47 (2017).

[27] Pickles, A. J., Young, T. T., Nakamura, W., Cowie, L. L., Graves, J. E., Jim, K. T. C., Keller, T. J., Luppino, G. A., Northcott, M. J., Roddier, C. A., Stockton, A. N., Wainscoat, R. J., Yamada, H., and Cavedoni, C. P., "UH/IfA Fast Tip-Tilt Secondary," in [*1994 Symposium on Astronomical Telescopes & Instrumentation for the 21st Century*], (June 1994), 504–515 (1994).

[28] Hemmati, H., [*Deep Space Optical Communications*], Deep Space Communication and Navigaton Series, Issued by the Deep Space Communications and Navigation Systems Center of Excellence Jet Propulsion Laboratory California Institute of Technology (2005).

[29] Munning Schmidt, R., Schitter, G., Rankers, A., and Van Eijk, J., [*The Design of High Performance Mechatronics*], Delft University Press, Amsterdam, 2nd ed. (2014).

[30] Jabben, L. and Van Eijk, J., "Perfomance analysis and design of mechatronic systems," *Mikroniek* **51**(2), 5–12 (2011).

[31] Csencsics, E. and Schitter, G., "System Design and Control of a Resonant Fast Steering Mirror for Lissajous-Based Scanning," *IEEE/ASME Transactions on Mechatronics* **22**(5), 1963–1972 (2017).

[32] Hemmati, H., [*Near earth laser communications*], CRC Press, New York (2009).

Pre-print version of the article: A. Sinn, T. Riel, P. Kremsner, and G. Schitter, "Analysis of tip-tilt compensation for reflective free-space optical satellite communication," *Free-Space Laser Communications XXXI,* 109101G, 2019. DOI: 10.1117/12.2506472

[33] Tyler, G. a., "Bandwidth considerations for tracking through turbulence," *Journal of the Optical Society of America A* **11**(1), 358 (1994).
[34] Noll, R. J., "Zernike polynomials and atmospheric turbulence," *Journal of the Optical Society of America* **66**(3), 207 (1976).
[35] Jian, H., Ke, D., Chao, L., Peng, Z., Dagang, J., and Zhoushi, Y., "Effectiveness of adaptive optics system in satellite-to-ground coherent optical communication.," *Optics express* **22**(13), 16000–7 (2014).
[36] Hardy, J. W., [*Adaptive optics for astronomical telescopes*], Oxford University Press, New York (1998).

Pre-print version of the article: A. Sinn, T. Riel, P. Kremsner, and G. Schitter, "Analysis of tip-tilt compensation for reflective free-space optical satellite communication," *Free-Space Laser Communications XXXI,* 109101G, 2019. DOI: 10.1117/12.2506472